The Journal of Korean Vacuum Science & Technology
Vol. 2, No. 2, October 1998, pp. 63~77

Growth of γ-Al_2O_3 (111) on an ultra-thin interfacial Al_2O_3 layer/NiAl(110)

M. B. Lee, B. G. Frederick† and N. V. Richardson‡

School of Electronic and Electrical Engineering
University of Kyungpook National University, Taegu, 702-701, Korea
†Department of Chemistry, University of Maine, Orono, ME, 04469, USA
‡School of Chemistry, University of St Andrews, St Andrews, KY16 9ST, Scotland
(Received July 3, 1998)

Abstract – The oxidation of NiAl(110) was investigated in the temperature regime between 300 K and 1300 K using LEED (low energy electron diffraction), TPD (temperature programmed desorption) and HREELS (high resolution electron energy loss spectroscopy). The adsorption of N_2O and O_2 up to saturation on NiAl(110) at 300 K only leads to the selective oxidation of surface aluminium without reconstructions. Stepwise annealing of the oxygen-saturated sample from 600 K to 1300 K in UHV (ultra-high vacuum) results in firstly the onset of randomly oriented then finally fairly well-ordered, 5 Å Al_2O_3 film with quasi-hexagonal periodicity. Ordered thicker oxide films of 18-30 Å seem to be grown on this interfacial oxide layer by direct oxidation of sample at elevated temperatures between 1150 and 1300 K because of the LEED pattern consisting of new broad hexagonal spots and the previous 5 Å spots. Although the periodicity of surface oxygen arrays shows no significant change from an hexagonal close-packing, the O-O distance changes from ~3.0 Å for the 5 Å film to ~2.9 Å for thicker oxides. With the appearance of Auger parameter, for the 5 Å film, which is significantly different from those of γ- and α-like Al_2O_3 samples, the 5 Å film can be described better as an *interfacial oxide* layer. The observation of three symmetric phonon peaks can be also a supporting evidence for this phase assignment since thicker oxide films on the same NiAl(110) show somewhat different phonon structure much closer to that of the γ-Al_2O_3. The adsorption/desorption of methanol further proves the preparation of less-defective and/or oxygen-terminated Al_2O_3 films showing ordered phase transitions with the change of oxide thickness between 5 Å to 30 Å.

1. Introduction

The spectroscopic investigation of the oxidation of metal surfaces and the oxides themselves has traditionally been considered of major research interest in surface science due to its importance in many applications such as metallurgy, corrosion, electrochemistry, catalysis and electro-optical technology [1]. Metal oxides, which can be classified into transition and non-transition metal oxides, have been extensively studied to elucidate the electronic, structural and vibrational properties using many surface-sensitive spectroscopic facilities. Some transition metal oxides reveal phase transitions from a metallic to a non-metallic state as a function of temperature, pressure or composition [2]. In view of the catalytic applications, the surface properties of conducting or semiconducting transition metal oxides have been examined using HREELS [3-8], XPS and AES [9-12] and LEED and STM (scanning tunneling microscopy) [13, 14].

Of non-transition metal oxides, the most widely and intensively investigated is aluminium oxide. From studies on alumina-supported model catalysts [1, 15-18], serious complications can arise from the amorphous or polycrystalline nature of transition phase aluminium oxide samples. The adsorption of molecules may be different on highly defective and incompletely oxidised alumina sur-

faces than on perfect crystals [19, 20]. When metals or metal carbonyl clusters are deposited onto Al_2O_3/Al [21, 22], the underlying Al stimulates the deposition and the inward diffusion of the deposited metal probably via grain boundaries and forms an alloy which may have different catalytic behaviour. Furthermore, charging problems [23, 24] have severely limited the application of surface-sensitive techniques to bulk oxide materials since most rely on electrons or ions to gain surface specificity. Sample heating and cleaning are also serious difficulties generally encountered for bulk oxides due to the poor electrical and thermal conductivities of these materials. An alternative method to circumvent these problems is to use ultra-thin oxide films instead of bulk oxides [25, 26]. Therefore, the preparation of well-ordered and defect-free aluminium oxide thin films is critical for understanding not only the physical and chemical role of oxide film but also that of surface defects if the thin film approach is to be successful.

It is generally accepted that direct oxidation of Al^0 generally produces amorphous and/or polycrystalline γ-phase alumina films [27] with ill-defined surfaces and interfaces [28]. Moreover, the presence of metallic Al^0 species in oxide films seems to be an additional difficulty for the reliable interpretation of spectroscopic data as previously pointed by Chen *et al.* [19]. In contrast, the use of different refractory metal substrates for the synthesis of alumina films has provided scientists with more flexibility required for the selective and reliable growth of alumina films with relatively well-defined surfaces and interfaces by depositing Al^0 films either in high vacuum or controlled oxygen environment followed by heat treatment to high temperature. Pseudo-hexagonal Al_2O_3 overlayers of 5-40 Å was prepared on a Ta (110) substrate between 700 and 900 K by vacuum reactive Al deposition in an oxygen flux [29]. Long-range ordered Al_2O_3 films with an hexagonal periodicity were prepared on Ru(0001) and Re(0001) via Al deposition in an oxygen environment at elevated temperatures [30]. Similar hexagonal periodicity has been observed for the ultrathin oxide films prepared by two-step deposition/oxidation of Al on Ru(0001) [31, 32].

In addition, the oxidation of NiAl single crystals has resulted in a fairly well-ordered aluminium oxide thin films on three primary surfaces, (100), (110) and (111). The selective growth of a fairly well-ordered pure alumina overlayer with an hexagonal periodicity was firstly reported on NiAl(111) via oxygen adsorption/annealing [33]. Most recently, Franchy *et al.* [34] reported the phase transition and facetting of an ordered alumina overlayer for the annealing temperature over 1100 K. Gassmann *et al.* [35] reported phase transitions of alumina films with increasing oxide thickness from ~8 Å to 20 Å on NiAl(001). Following the preparation of epitaxially grown oxide films, by oxygen adsorption and annealing at substrate temperatures of 1200-1300 K (20 Å), combined HREELS, LEED and AES techniques were employed to monitor the phase transitions from the γ-like to θ-like aluminium oxide films. On NiAl(110), Isern and Castro [36] also found that oxygen uptake stops with formation of a long-range, well-ordered Al_2O_3 film with a self-limiting thickness of ~5 Å. Most of the recent oxidation studies of a NiAl(110) surface [37-39] have confirmed the epitaxial growth of a long-range ordered 5 Å thick Al_2O_3 superstructure, and a bulk-like γ-Al_2O_3(111) or α-Al_2O_3(0001) structure was proposed as a probable structure because of its quasi-hexagonal oxygen periodicity [37]. No studies have been made on the epitaxial growth of thicker aluminium oxide films on this NiAl(110) surface. Therefore, the synthesis of thicker, ordered Al_2O_3 films on the same NiAl(110) surface described here should pro-

vide both useful electronic, structural and vibrational information for the better understanding of ultra-thin aluminium oxide surface and interface properties and better model supports for catalytic studies.

In this study, we have pursued similar approach for the preparation and characterisation of fully oxidised, well ordered, ultra-thin Al_2O_3 overlayers, in the thickness range of 5-30 Å on a single crystal NiAl(110) surface as a function of substrate temperature. Firstly, for comparison with previous results, HREELS and LEED data of the ultra-thin, 5 Å Al_2O_3 film are measured and correlated with Auger and photoemission data. Secondly, the oxide thickness-dependent electronic, structural and vibrational properties of these alumina surfaces have been systematically explored using combined AES, XPS, LEED, TPD and HREELS techniques. For convenience, only LEED and TPD/HREELS results are presented in this article and two separate papers are in preparation to elucidate a probable origin of the oxide thickness-dependent chemical shifts and three (or four) vibrational features of ultra-thin Al_2O_3 films. According to this study, the 5 Å well-ordered oxide film on NiAl(110) can be better described as an *interfacial oxide layer* with quasi-hexagonal oxygen arrays rather than γ- or α-like Al_2O_3 film and support for this view was provided by observations both that well-ordered aluminium oxide films of 10-30 Å thickness range can be grown on top of the 5 Å oxide/NiAl(110) and that the Auger parameter of the 5 Å film was largely different from those of γ- and α-Al_2O_3. The ordered phase transition of oxide overlayers has been also observed with the increase of film thickness from 5 Å to $\geq$18 Å. The experimental details are discussed in Section II and Section III includes the key experimental results. The interpretation and/or discussion appears in Section IV and summaries are given in Section V.

2. Experimental

This investigation was carried out in a two level, stainless steel, UHV apparatus with surface preparation facilities and many *in-situ* characterisation tools such as LEED, AES, XPS, TPD and HREELS. Details of the used system are given in elsewhere [32] but in this article, a brief description will be made for the key spectroscopic tools. The upper part of the main chamber is equipped with an Ar^+- ion gun of 500 eV (VSW AS10) for cleaning of the sample. LEED (Omicron SpectaLEED) was used for the structural characterisation of clean NiAl(110) substrate and the alumina thin films. A translatable stainless steel doser of 0.125" diameter allows one to achieve higher local gas pressure near crystal surface and, for residual gas analysis and TPD experiment, a high-speed, pulse counting quadrupole mass spectrometer (Hiden HAL II) was used.

A rotatable, single-stage hemispherical analyser (VSW HA50) was used for angular dependent AES, XPS and HREELS experiment with a source of an electron gun (VSW EG5), a twin anode, non-monochromatised X-ray source (PSP TA10) and a fixed, single stage electron monochromator (VSW monochromator). Auger spectra were recorded using pulse counting detection in the N(E) mode at a primary beam energy of 2.5 kV. Vibrational EEL spectra were collected in a specular direction at various scattering angles with respect to the surface normal and incident beam energies of 5-30 eV. The analyser was calibrated to the binding energies of the Au $4f_{7/2}$ (83.8 eV) and Ag $3d_{5/2}$ (367.9 eV) levels of clean samples which were spot-welded on the bottom of the sample manipulator and most of measurements was made near 300 K in an UHV of $1\text{-}3\times10^{-10}$ mbar range. Typical resolution (full width at half maximum) of the elastic peak for HREELS is 60-70 cm^{-1} for a well-ordered

alumina surface on NiAl(110). LEED images were captured using a CCD camera and frame grabber card (High Resolution Technologies HRT512-8) in an MS-DOS PC.

A clean NiAl(110) is obtained by repeated cycles of Ar^+-ion sputtering at 1.5 KeV (1 KeV negative sample bias) and annealing at a temperature of 1300 K in UHV. The cleanness is determined by combined AES/XPS, LEED and HREELS measurements revealing only the metallic Al and Ni Auger lines/core levels, centred rectangular (1×1) unit cell and a Ni-Al phonon branch at the loss energy of 220 cm^{-1}. In fact, since the alloy β-NiAl has a high melting point of 1640°C, low density of 5.86 g/cm^3 and high elastic constant of 296 GPa [40], it is a suitable material for high-temperature applications. For study, we have used a NiAl(110) single crystal with a surface area and thickness of 7×10 mm^2 and 1.0 mm as a substrate. For oxygen adsorption on a pre-cleaned NiAl, two different types of oxygen source, i.e., O_2 and N_2O, were employed and tested to better prepare ultra-thin aluminium oxide films. The background N_2O and O_2 pressure during dosing was normally about $1\text{-}2\times10^{-6}$ mbar and oxygen adsorption to saturation coverage was mainly determined by an annihilation of substrate spots in LEED. Extended annealing of oxygen saturated NiAl(110) surface to 1250-1300 K for about 5-10 min revealed a previously reported, typical LEED pattern [37] and will be referred to as the "5 Å" oxide film. In particular, thicker, 18-30 Å oxide films were epitaxially grown by higher temperature oxidation and annealing of the NiAl(110) sample with or without a 5 Å oxide film. The oxide thickness was determined by the measured relative ratio of the oxide-related Al^{3+} to the metallic Al^o KLL Auger transitions, assuming a uniform overlayer thickness. After the subtraction of linear background from each Al KLL Auger spectrum as typically shown in Figure 2, the least-square fitting process has been applied to obtain the integrated area of Al^o and Al^{3+} KLL Auger peaks. Since the Al^o KLL Auger intensity was almost completely attenuated for the oxide surface thicker than 25 Å, the oxide thickness of 30 Å was approximately determined by considering the relative change of Al^{3+} peak intensity and oxidation conditions.

3. Results

3.1 LEED Results

Once a clean, long-range well-ordered NiAl (110) surface was prepared, oxygen adsorption was carried out through a gas doser at room temperature using either dry O_2 or N_2O. The substrate LEED spots were degraded with extended exposure to N_2O at a pressure of 2×10^{-6} mbar. With the elapse of dosing time, the substrate LEED spots became more diffuse without the appearance of extra spots and then, completely faded away. While about 1200 L O_2 adsorption at RT was confirmed to be a saturation exposure in good agreement with the previous studies [37, 39], N_2O adsorption required exposures $\geq$2000 L for saturation at 300 K as shown in Fig. 1a. After $\geq$2000 L N_2O dose, the substrate LEED spots were not visible any more and XPS/AES for this surface showed no evidence for nitrogen adsorption.

Although greater N_2O exposure, compared to O_2, was required for saturation, both the O_2 and N_2O saturated NiAl(110) surfaces revealed similar thermal behaviour upon subsequent annealing at temperatures from 600 K to 1300 K. In LEED, firstly, with the increase of annealing temperature to 600 K, the substrate spots reappeared accompanied by a diffuse ring structure with an average reciprocal vector of ~2.40 $Å^{-1}$. Secondly, the substrate spots became more intense and the diffuse ring began to break into six major fragments by annealing to 1000 K (Fig. 1b). Finally, further annealing to 1300 K led to the final LEED pattern shown in Fig. 1c. Similar ring

structures have been observed in previous oxygen adsorption experiments [37, 39] and Xe-adsorption experiments on NiAl(110) at 50 K [41]. On this basis, the appearance of this ring structure was considered to indicate epitaxial growth of an aluminium oxide overlayer with distinct domains of hexagonal long-range order but randomly oriented with respect to the underlying NiAl substrate.

The appearance of the sharp LEED pattern (Fig. 1c) has been regarded as the final stage of oxidation and ordering. In order to further check the periodicity of the surface structure of Fig. 1c, LEED patterns were recorded at various incident energies from 8 eV to 250 eV and careful examination of these patterns revealed that the 5 Å film consisted of two equivalent domains, corresponding to a quasi-rectangular unit cell of a= 10.55 Å, b=17.88 Å, α=88.7° in real space [37, 39], rotated by ±24.1° from the <110> axis. The clear presence of substrate LEED spots suggests that the ultra-thin, well-ordered overlayer should generate doubly diffracted LEED spots as identified by SPA-LEED [39].

Besides, AES/XPS and HREELS results support the epitaxial growth of the well-known, ultra-thin and extremely well-ordered Al_2O_3 film of 5 Å thickness by oxygen adsorption on a precleaned NiAl(110) up to saturation at 300 K (or 550 K) followed by subsequent annealing at 1300 K in UHV [37]. In addition, we have prepared thicker oxide films on the same NiAl(110) substrate in a thickness range of 18-30 Å by high-temperature (1150-1300 K) oxidation in the N_2O and O_2 pressure of 2×10^{-6} mbar. Measured AES spectra are given in Figure 2 for various surface oxide thicknesses. These overlayer films revealed new

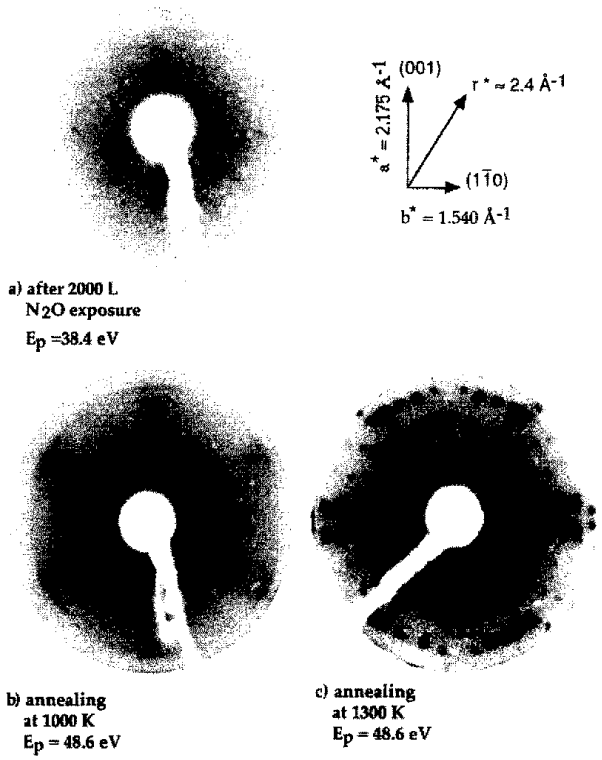

Fig. 1. LEED patterns of a) quasi-oxygen saturated surface at 300K, b) and c) after annealing for 10 min at 1000K and at 1300K in UHV.

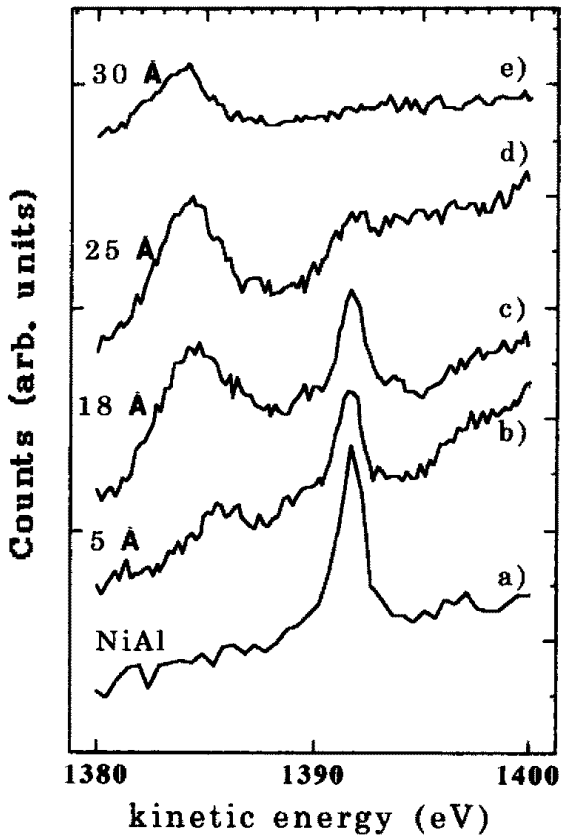

Fig. 2. Al KLL Auger spectra indicating the relative intensity change between the Al^0 and Al^{3+} peaks grown on the same NiAl(100) substrate. The correpsonding aluminum oxide thickness is marked near each spectrum of a) clean NiAl(100), b) 5 Å, c) 18 Å, d) 25 Å and e) ~30 Å.

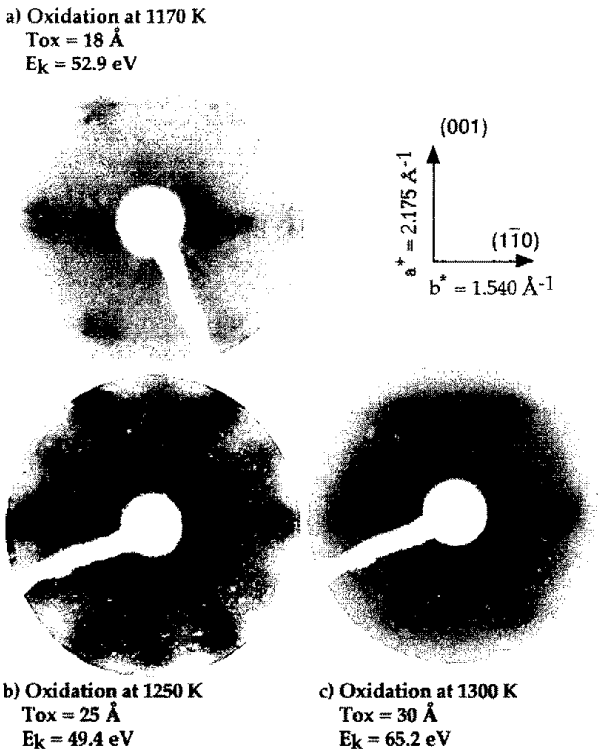

Fig. 3. LEED patterns showing a transformation of overlayer structure with the growth of thicker aluminium oxide films on NiAl(110). Each oxidation temperature, overalyer thickness and primary electron energy are marked in each pattern of a), b) and c).

electronic, structural and vibrational properties but, to some extent, related to the 5 Å alumina film on the same NiAl (110) substrate.

Fig. 3 illustrates the observed LEED patterns showing a transformation of overlayer structure, from a) a broad hexagonal, b) 12-directional to c) 12-directional spots for film thicknesses of 18, 25 and 30 Å, respectively. The 18 Å overlayer gave rise to some spots which, can be attributed to the underlying 5 Å interfacial layer between the NiAl substrate and thicker Al_2O_3 overlayer or to the growth of oxide islands due to the limited diffusivity of aluminium or oxygen.

The key oxidation parameter in obtaining thicker aluminium oxide films was temperature in a constant oxygen environment of 2×10^{-6} mbar. Each overlayer was obtained by 20 min oxidation followed by subsequent annealing in UHV at the indicated temperatures, 1170, 1250 and 1300 K. In the present experiment, high-temperature oxidation of the NiAl(110) substrate was not dramatically influenced by prior formation of the 5 Å well-ordered overlayer. In fact, no further oxygen uptake by NiAl(110) substrate with the 5 Å film was possible below 1100 K since the surface structure of NiAl(110) covered with the 5 Å Al_2O_3 thin film did not change with the elapse of oxidation time. This observation might be strongly related to the crystallinity of the 5 Å film with its high degree of structural perfection resulting in a very limited diffusion of oxygen or Al atoms via domain boundaries. The overall LEED analysis of thicker films revealed an average oxide domain size of 40-45 Å with a surface periodicity of 2.9 ± 0.1 Å assigned to an average oxygen-oxygen distance within hexagonal close-packed oxygen arrays and seemed to support an epitaxial growth of thicker aluminium oxide films on the interfacial, 5 Å Al_2O_3 film.

However, the appearance of relatively sharp NiAl substrate spots in the 18 Å Al_2O_3 thin film is difficult to understand on the basis of a uniform oxide overlayer since the substrate contributions should be almost attenuated for the primary electron beams of 60-70 eV with an inelastic mean-free path of ~10 Å in Al_2O_3. Since LEED measurements of the 25 Å overlayer film changed dramatically as the sample cooled after annealing in UHV, from 380 to 302 K, we can expect, from the electron mean-free path consideration in an Al_2O_3 film, that LEED patterns of 25 and 30 Å thick overlayers would show only overlayer spots for the incident electron beam of 71.0 eV. Therefore, as recently reported from a temperature-dependent LEED study of Cr_2O_3(111)/Cr(110) [42], the sharper, brighter substrate spots at higher temperatures could be due to temperature-dependent structural changes of the top surface layer in thin films although surface diffusion of aluminum atoms would normally be expected at much higher temperatures.

3.2 Methanol Adsorption / Desorption Results

Fig. 4 illustrates the corresponding thermal desorption spectra of the major 31 amu mass fragment for several coverages of methanol adsorbed on A) the perfectly well-ordered 5 Å interfacial oxide overlayer and B) the 25 Å oxide film on the same NiAl(110) surface at 131 K. In this experiment, the fragmentation of desorbed methanol as well as gas phase methanol in UHV has revealed similar spectra, for key masses 32, 31, 30, 29 and 15 amu, which are in close agreement with the published cracking patterns [43]. For the case of the 5 Å film given in Fig. 4 A), a weakly chemisorbed submonolayer peak begins to appear near 250 K for an extremely low coverage (0.0025 L) dosed for 5 sec at the methanol background pressure of 5×10^{-10} mbar. For the methanol exposures between 0.06 L (spectrum b) and 0.1 L (spectrum c), the maximum temperature of this asymmetric desorption peak shifts down to ~220 K followed by a subsequent increase of peak intensity (or area). With the further increase of methanol exposure to 0.16 L (spectrum d) and 0.2 L (spectrum e), the weakly chemisorbed asymmetric desorption peak shows a systematic increase of peak intensity accompanied by a further shift down of maximum desorption temperature to ~197 K for 0.16 L and to ~183 K for 0.2 L without a clear appearance of new peaks. Thicker oxide films of 18-30 Å range have also shown the equivalent thermal desorption spectra to those of the 5 Å oxide overlayer for similar methanol exposures and the experimental results for 25 Å γ-Al_2O_3 surface are depicted in Fig. 4 B). For low methanol exposures of 0.01 L (spectrum a), only a chemisorbed submonolayer desorption peak appears at ~200 K. The maximum desorption temperature shifts down and saturates near ~180 K accompanied by the gradual saturation of peak intensity as the methanol exposure increases from 0.07 L to 0.3 L (spectrum b, c and d) without a distinct indication for the occurrence of new peaks.

In contrast, the thermal desorption spectra of much higher methanol exposures have consistently revealed a gradual saturation of both peak desorption temperature near ~175 K and peak intensity with the simultaneous development

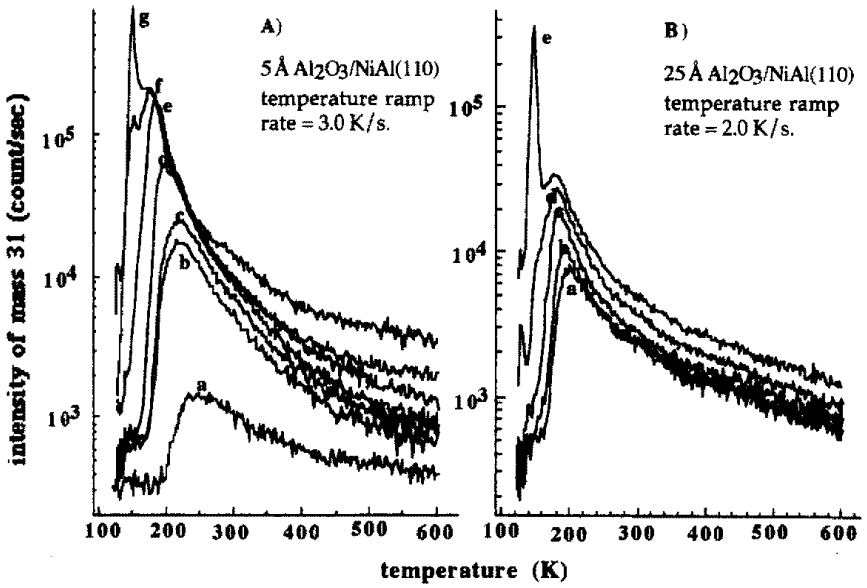

Fig. 4. Thermal desorption spectra A) for a) 0.0025 L, b) 0.06 L, c) 0.1 L, d) 0.16 L, e) 0.2 L, f) 0.5 L, g) 1 L methanol on the long-range, well-ordered 5 Å Al_2O_3 interfacial layer on NiAl(110) and B) for a) 0.01 L, b) 0.07 L, c) 0.1 L, d) 0.3 L, e) 1 L methanol on the long-range, well-ordered 25 Å γ-Al_2O_3 films on NiAl(100). Adsorption temperature T_{ads} = 131 K, adsorption pressure range = 5×10^{-10}-1×10^{-8} mbar.

of an additional peak centred at a fixed desorption temperature of ~150 K. As depicted in Fig. 4, a sharp and symmetric desorption peak starts to appear at ~150 K for 0.3-0.5 L and becomes a dominant feature for 1.0 L, while the latter desorption peak gradually increases without saturation of peak intensity for greater exposures. This latter symmetric desorption peak should be regarded as a physisorbed multilayer desorption feature since not only the peak intensity continuously increases without saturation but also the maximum desorption temperature doesn't distinctively shift down or up for much greater methanol exposures. Then, the formation of methanol multilayer can be assumed to occur only after the completion of the first monolayer adsorption roughly corresponding to the exposure of ~0.2 L at the adsorption temperature of ~130 K. In this point of view, the shift down of the maximum desorption temperature from 250 K to 175 K can be attributed to the existence of the strong lateral interactions [44, 45] between the randomly chemisorbed methanol clusters or islands up to a monolayer coverage.

To further check the nature of this weak submonolayer chemisorption state, the HREEL spectrum of each oxide surface has been recorded for a submonolayer methanol coverage dosed by ~0.2 L at 131 K. Fig. 5 shows the corresponding HREEL spectra of the long-range, well-ordered 5 Å interfacial oxide layer with its typical three phonon loss features (spectrum a) and the same oxide surface after adsorption of 0.2 L methanol at 131 K (spectrum b). By assuming 0.3 L exposure at 131 K as a monolayer coverage, 0.2 L exposure at the same temperature was estimated to be about 0.83 ML coverage from the relative area ratio analysis of the corresponding thermal desorption spectra as depicted in Fig. 3. The difference between the HREEL spectra of the clean oxide surface and the 0.2 L methanol dosed oxide surface revealed four (or five) dominant vibrational

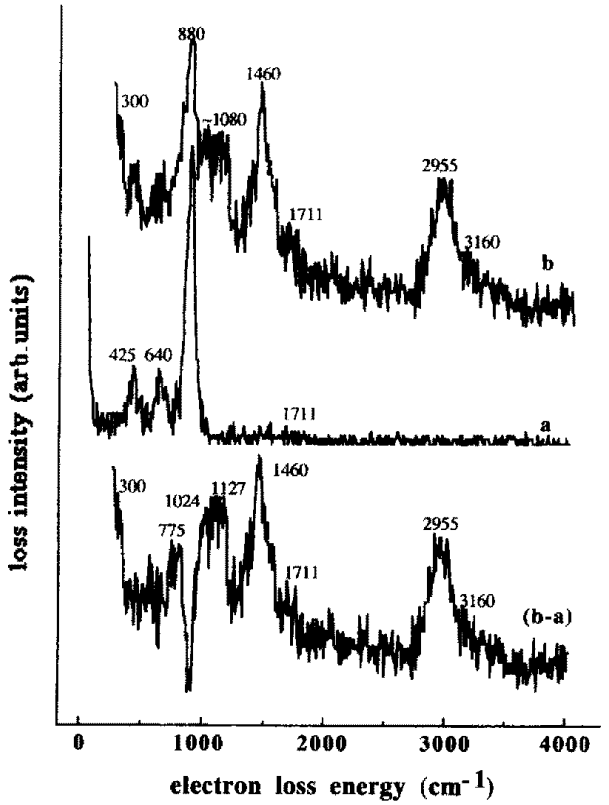

Fig. 5. HREEL spectra for submonolayer adsorption of methanol on the 5 Å interfacial oxide layer on NiAl(110) at 131 K and (b-a) difference between two spectra, a and b, $E_p = 10$ eV, $\theta_i = \theta_f = 40°$.

features at ~775, ~1080 (two modes), ~1460 and ~2955 cm^{-1}. By comparing the frequencies of the solid phase CH_3OH [46], molecularly adsorbed CH_3OH on Al(111) [47] and CH_3OH on Al_2O_3 thin film on Ru (0001) [48], as given in Table 1, one can correctly assign four overlayer-related vibrational modes to molecularly adsorbed methanol species on the long-range, well-ordered Al_2O_3 thin films on NiAl (110).

4. Discussion

4.1 N_2O Adsorbed NiAl(110) Surface

Compared to the other low-index surfaces showing p(1×1) or reconstructed $c(3\sqrt{2}\times\sqrt{2})R45^0$ structures according to annealing conditions [49], no reports have been made of surface reconstruction of this NiAl(110) surface [49-53]. Thus, the appearance of extremely sharp LEED spots up

Table 1. Vibrational frquencies (cm^{-1}) of solid phase CH_3OH(s) [46], CH_3OH/Al(111) [47], $CH_3OH/Al_2O_3Ru(0001)$ [48] and submonolayer (~0.83 ML) $CH_3OH/Al_2O_3NiAl(110)$.

Mode	CH_3OH(s)[a]	CH_3OH/Al(111)[b]	CH_3OH/Al_2O_3[c]	CH_3OH/Al_2O_3[d]	
ν (Al-O)	–	485	–	–	
δ (OH)	730	675-760	–	775	
ν (CO)	1032	1010	1020-1040	1024	1080
γ (CH_3)	1124	1145	–	1127	
ν_s (CH_3)	1452	1475	1445	1460	
ν_{as} (CH_3)	2828	–	–	2800	
ν (OH)	2951	2690	2930	2955	2955
	3225	3220	3100	3160	

a) From ref. [46], b) ref. [47], c) ref. [48] and d) present study.

to an electron energy of 200 eV was considered as an indication of a clean, well-ordered and bulk-truncated NiAl (110) surface (although the Ni/Al vertical corrugation is 0.22 Å). The two-dimensional unit cell was readily determined to be 2.89×4.08 Å^2 from the observed positions of LEED spots along each direction. This agrees well with the $(a\times\sqrt{2}a)$ on the basis of the bulk lattice constant (a) of 2.89 Å.

No ordered surface reconstruction occurred with both the N_2O and O_2 adsorption up to the saturation on a clean NiAl(110) surface at the substrate temperature range of 300-600 K. Without any effects by the atomic nitrogen, only atomic oxygen species were dissociatively adsorbed and selectively interacted only with Al atoms to form Al_2O_3 species. Instead, with increase of N_2O adsorption on a clean NiAl(110) surface near 300 K, only a gradual attenuation of substrate LEED spots was observed upto saturation coverage at an exposure of ~2000 L N_2O. While the O_2 dose for saturation was ~1200 L [37], the required N_2O dose was about 67% higher than O_2 dose. This increase of the saturation exposure seems to be consistent with the available oxygen atoms per molecule, two oxygens from O_2 dissociation and one oxygen from N_2O dissociation. In a sense, the 67% increase may also reflect a difference of bond strength between two gases. Since the heat of formation is 82.1 KJ/mol for N_2O [54] which is by a factor of three smaller than the corresponding value of 249.2 KJ/mol for O_2 gas [54], one might expect an extra-enhancement of the oxygen density at the gas-solid interface for N_2O gas with respect to O_2 gas at the same adsorption conditions.

The disappearance of the substrate LEED spots at higher N_2O doses, accompanied by the strong enhancement of background intensity, is due to the surface disordering within the depth of about 5-7 Å which is equivalent to the mean free path of the low energy electron beam [55]. Since the NiAl(110) has a layer spacing of 2.04 Å two- or three top layers of NiAl corresponding to 4.08-6.12 Å range can be assumed to be affected by the nitrous oxide adsorption up to the saturation coverage. Moreover, since the surface Al net of the NiAl(110) surface corresponds to a rectangular unit cell of 2.89×4.08 Å^2 almost identical to the 2.86×4.05 Å^2 of an Al(110) surface [56], the NiAl(110) surface might be expected to mimic the oxygen uptake behaviour of this single crystal Al surface. In fact, since the Al(110) surface shows direct formation of aluminium oxide rather than a stable chemisorption at 300 K [56], the oxygen uptake behaviour of the NiAl(110) surface seems to be more or less compatible with that of the Al surfaces. Also, if the atomic oxygen randomly adsorbs on the surface, the degradation of the substrate LEED pattern will be accelerated. On this basis, the initial degradation of the NiAl(110) substrate LEED spots with the extended nitrous

oxide exposure can be attributed to a probable rearrangement of Ni and Al atoms within top two or three surface layers.

The appearance of the diffuse ring structure followed by breaking-up into six ring segments would be characteristic of an adsorbate layer with distinct domains of long-range order but random orientation with respect to the underlying NiAl substrate. A comparable LEED pattern with six ring segments was observed from the Xe adsorption on NiAl(110) at 50 K [41] and explained by a structural model consisted of three domains randomly oriented with respect to NiAl (110). By assuming the Ni rows as the preferred adsorption sites for Xe, two hexagonal close-packed extra-domains were identified to produce the six ring segments LEED pattern which were in good agreement with the Xe-induced overlayer LEED structure. In the other domain, Xe atoms were postulated to be one-dimensionally condensed along the Ni rows and also the existence of slightly rotated Xe overlayer was evidenced by the appearance of the elongated line structure. In the same point of view, the appearance of the ring structure followed by six ring segments can be understood by the two or three randomly oriented (but favourable to the condensation along (001) direction) Al_2O_3 domains with a close packed hexagonal periodicity.

Nevertheless, there exist two distinctive differences between the Xe-induced and Al_2O_3-induced overlayer LEED patterns on NiAl(110) surface; one is the orientation which the elongated lines appear and the other is the commensurate direction between the substrate and the overlayer LEED patterns (see Fig. 1). Two elongated lines of six segments match well with the (110) direction of the substrate for the Xe-induced LEED pattern and, in contrast, with the (001) orientation of the NiAl substrate for the Al_2O_3-induced LEED structure. In addition, the commensurate orientation varies from the (110) direction for the Xe adsorption to the (001) direction for the nitrous oxide (or oxygen) adsorption. However, both differences are strongly relevant to the change of the local periodicity largely dependent on the atomic size of the adsorbates on the basis of the quasi-hexagonal close-packed overlayer formation. The distance between the first nearest neighbour Xe atoms and the first nearest neighbour O atoms in various Al_2O_3 phases is 4.48 Å [41] and 2.6-2.8 Å [57], respectively. Then, the close-condensation along the (001) direction with a periodicity of 2.89 Å rather than the (110) direction with a corresponding value of 4.08 Å is most favourable to the Al_2O_3 overlayer on the NiAl(110) surface. Still, it is not easy to establish a structural model for this transient ring structure partly due to the formation of Al_2O_3 via the Ni diffusion into the bulk NiAl rather than a simple adsorption of the adsorbate.

However, the average local periodicity of the randomly oriented domains can be easily gained from the average radius of the observed ring structure. Therefore, in the ring structure with the hexagonal local periodicity, the reciprocal radius of ~2.40 $Å^{-1}$ estimated from the relative substrate spot position can be correlated to the average lattice constant of ~3.0 Å which is in good accordance with the results of the previous studies using LEED [37] and SPA (spot-profile-analysis)-LEED/STM [39]. This lattice constant is much closer to the corresponding O-O distance of 2.6-2.8 Å range rather than the larger periodicity of most crystalline alumina phases. Thus, to a good approximation, the oxide domains on NiAl(110) can be described to be terminated by quasi-hexagonal close-packed oxygen arrays.

4.2 Surface Periodicity of Al_2O_3 Films on NiAl(110)

As evidenced by the observation of perfectly well-resolved, overlayer-induced LEED pattern with sharp substrate spots, the thermal treatment

up to 1300 K seems to continuously improve both the crystalline properties of the overlayer and the interface between the overlayer and the substrate. The final Al_2O_3-induced LEED pattern for the N_2O gas (Fig. 1c) was in good resemblance with the results of previous studies for O_2 gas [37-39]. The overlayer has been continuously identified to be a stoichiometric, well-ordered 5 Å Al_2O_3 film corresponding to the two Al-O layers and also the clear appearance of the substrate spots with overlayer spots seems to be compatible with this oxide thickness considering the inelastic electron mean free path. Thereafter, the final overlayer structure was called as "5 Å film". As a most likely structure of 5 Å film, Muller *et al.* [58] presented the two-dimensional real-space unit mesh with the structural parameters, a = 10.55 Å, b = 17.88 Å and $\alpha = 88.7^\circ$ which is much larger than that of NiAl(110), a = 2.887 Å, b = 4.08 Å and $\alpha = 90^\circ$ [50, 59]. The existence of two equivalent overlayer domains was assumed due to the C_{2v} symmetry of the NiAl(110) substrate and identified to be rotated by $\pm 24.1^\circ$ with respect to the (110) orientation of the substrate by LEED [37, 58] and STM [39].

According to this model, the local periodicity of the 5 Å film along the (110) orientation (4.11 and 16.34 Å) well matches with the corresponding one of the NiAl(110) substrate (4.08 Å) within the error of less than 1% but the equivalent periodicity along (001) orientation (9.77 and 7.31 Å) largely mismatches with that of the NiAl(110) substrate (2.89 Å). Thus, the 5 Å overlayer film can be concluded to be "*commensurate*" with the underlying NiAl(110) along the (110) direction but "*incommensurate*" along the (001) direction. Here, one can also note the variation of the commensurate direction from the (001) for the ring structure to the (110) direction for the final 5 Å oxide film. In thermodynamic point of view, one can speculate that the misaligned overlayer structure with respect to the NiAl(110) surface may be rather stable configuration than the simple condensation along both direction of NiAl(110). From the optimum temperature of ~1300 K, an energy barrier of ~0.11 eV can be attributed to the onset of the long-range, well-ordered 5 Å oxide film on the NiAl(110) substrate. To large extents, the model well simulates the experimental LEED patterns over a fairly wide range of electron beam energy so that the corresponding domain of each observed spot can be assigned by direct comparison with the model LEED pattern.

As shown in Fig. 3, with the subsequent increase of overlayer thickness up to 30 Å, Al_2O_3 films on the same NiAl(110) substrate revealed a thickness dependence of the surface structure. The aluminium oxide films of 18 Å (~7 ML), 25 (~10 ML) and 30 Å (~12 ML) have revealed a broad hexagonal, 12-directional and 12-directional LEED patterns, respectively. From the hexagonal LEED pattern of 18 Å thick aluminium oxide film, one may note a structured hexagon accompanied by substrate spots. A careful examination of the 5 Å and 18 Å oxide overlayer LEED patterns reveals that the 5 Å oxide overlayer is an accommodative, interfacial layer for the epitaxial growth of thicker films since the positions and internal structure of the hexagons are in good accordance with those of the most intense groups of the 5 Å oxide overlayer spots. In addition, since thicker oxide films prepared on NiAl with or without the 5 Å film have revealed the same broad hexagonal LEED spots, the formation of an interfacial oxide layer seems to be a prerequisite for the subsequent epitaxial growth of thicker oxide films on NiAl(110). Upon considering the 12-directional LEED patterns of the thicker oxide films (25 and 30 Å) on the quasi-hexagonal 5 Å oxide domain, it seems probable to guess coexistence of two hexagonal domains rotated by 30° (or 90°). The intensity deviation between the two sets of the hexagonal spots is not easy to explain but seems to be related to the

growth mechanism. Besides, certain degree of surface faceting due to high temperature oxidation of NiAl [35, 60] can be suggested as a probable reason. The two oxide domains turned out to have the O-O distance of ~2.90 Å.

Since the overlayer domain width (w) is an important structural parameter for the appearance of the broad LEED spots, it is crucial to reliably determine the average dimension of the flat area. In a simple way, the domain size can be calculated from the observed mean spot diameter (d) by using the following formula [61],

$$\frac{d}{s} = \frac{a}{w} \quad (1)$$

where s and a are the separation between two reference spots and the corresponding lattice constant, respectively. For the estimated parameters from the hexagonal broad LEED patterns with a mean lattice constant of 2.9 Å, the thicker oxide films have a mean size of about 40-45 Å, which is much smaller than that ($\geq$200 Å) [39] of the 5 Å oxide film. A similar domain size was also identified for the alumina film of ~24 Å grown on Ru(0001) [31, 32]. To a good approximation, the appearance of a limited domain size of 40-45 Å may reflect the transitional nature of thicker oxide films (probably γ-Al_2O_3) prepared on metal substrate and, in a highly surface-sensitive characterisation, a relatively thick transition alumina film surface may not readily illustrate any structural ordering despite of a certain crystallinity underneath.

4.3. Chemical Reactivity of Ultra-Thin Al_2O_3 Films on NiAl(110)

In order to characterise the chemical reactivity of the prepared various alumina surfaces including powder, bulk and thin film, temperature programmed thermal desorption (TPD) technique via the adsorption/desorption process of an appropriate molecular source has been widely employed solely or with the combination of the other surface-sensitive spectroscopic techniques so far [47, 48, 62, 63]. Similar TPD technique using methanol has been employed, in this study, to further investigate the presence of surface defects resulting in strong interactions between the adsorbed methanol and the alumina surface. However, up to the multilayer adsorption on the long-range, well-ordered Al_2O_3 thin films on NiAl(110) at the temperature range of 120-150 K, combined TPD and HREELS results have revealed only a simple molecular adsorption and desorption of methanol (CH_3OH) without a conceivable indication for relatively strong chemical modifications or dissociation.

For the extremely low coverage chemisorption peak, the leading edge analysis proposed by Habenschaden and Kuppers [64] indicated a desorption activation energy of ~29 KJ/mol for the 5 Å and thicker oxide films on the same NiAl(110) surface and turns out to be in excellent agreement with the previous study [48]. Thus, apart from a small temperature deviation between the methanol desorption spectra of the 5 Å oxide overlayer and 25 Å γ-Al_2O_3 film, two oxide surfaces with fairly long-range order can be assumed to show chemically inert surface properties. Distinct surface disordering of two oxide surfaces was not observed with this methanol adsorption and desorption process. To a good approximation, the observed desorption activation energy, 28-29 KJ/mol can be attributed to the fundamental strength of weak interactions between chemisorbed submonolayer methanol islands and well-oxidised alumina surface prepared in UHV rather than a surface defect-related chemisorption.

From the observation of relatively broad and/or asymmetric loss features in HREELS measurements of methanol adsorbed oxide surface, two vibrational features at 1080 and 2955 cm^{-1} can be assigned to two and/or three vibrational modes occurring at a similar frequency regime as

indicated in Table 1. In this point of view, one can assign the broad 1080 cm^{-1} loss feature to the overlapping of a CO-stretching mode, ν(CO) at ~1024 cm^{-1} and a CH_3-wagging mode, γ(CH_3) at ~1127 cm^{-1}. Further assignment can be made for the asymmetric loss feature of 2955 cm^{-1} to be relevant to three vibrational modes: a symmetric CH_3-stretching mode, $\nu_s(CH_3)$ at ~2800 cm^{-1}, an asymmetric CH_3-stretching mode, $\nu_{as}(CH_3)$ at 2955 cm^{-1} and a OH-stretching mode, ν(OH) at ~3160 cm^{-1}. The other two vibrational bands with relatively sharp and symmetric profile can be uniquely assigned to a OH-deformation mode, δ (OH) at 775 cm^{-1} and a CH_3-deformation mode, δ(CH_3) at 1460 cm^{-1}, respectively.

In addition to this principal vibrational bands, one can also expect some extra loss bands, with small relative intensities, relevant to the normal motion of the methanol molecule with respect to the substrate but, so far, no clear identification has been made. To a good approximation, the existence of the molecular loss features can be recognised from the strong intensity enhancement of the elastic tail near 200-350 cm^{-1} range as depicted in Fig. 5. Furthermore, the observation/ implication of the OH-stretching and-deformation modes supports the molecular adsorption. Therefore, one can finally conclude that CH_3OH is molecularly adsorbed, from the initial stage to multilayers, on the long-range, well-ordered and defectless Al_2O_3 films at 131 K.

5. Summary

In this study, long-range, well-ordered ultra-thin and less-defective Al_2O_3 films have epitaxially grown on a clean NiAl(110) surface; an interfacial layer of the 5 Å thickness is prepared via nitrous oxide (or oxygen) adsorption near room temperature followed by high temperature annealing in UHV and thicker films of 18-30 Å regime can be grown on this interfacial layer by direct high temperature oxidation between 1150-1300 K. A dissociative oxygen adsorption initially induces a local surface disorder with the oxygen dose to the saturation coverage (~1200 L for O_2 and ~2000 L for N_2O) near room temperature. With the increase of annealing temperature in UHV from 600 to 1150 K, the substrate spots initially reappear accompanied by a diffused ring structure with an average lattice constant of 3.02±0.08 Å and, then, become more intense and also the diffuse ring begins to break into six major fragments. The observed ring structure with an average lattice constant of ~3.02 Å is due to various hexagonal overlayer domains randomly oriented to the underlying NiAl(110) substrate. Furthermore, the surface termination of the oxide by quasi-hexagonal close-packed oxygen is indirectly evidenced by the observation of a larger lattice constant of 2.9 ~3.0 Å closer to the O-O distance of 2.6-2.8 Å rather than the Al-O distance of ~2.0 Å in the bulk Al_2O_3.

By annealing the oxygen saturated NiAl(110) surface at 1300 K, a perfectly well-ordered ultra-thin overlayer is consistently synthesised with a large unit cell, rotated by ±24° with respect to the NiAl substrate. The primary electron energy-dependent LEED patterns are in good agreement with the corresponding LEED structures simulated by using a previously reported quasi-rectangular overlayer unit cell (a = 10.6 Å, b = 17.9 Å, α = 88.7°) for the two equivalent domains relevant to the C_{2v} symmetry of NiAl(110) substrate. But, the 5 Å oxide overlayer surface may still maintain a distorted, local hexagonal oxygen symmetry with an average lattice constant of 3.01 Å which is in close accordance with the observed lattice constant of the diffused ring structure. Since the long-range ordered, 18 Å Al_2O_3 film shows the LEED pattern consisting of new broad hexagonal spots and the previous 5 Å spots both with hexagonal periodicity, the 5 Å oxide overlayer is considered as an interfacial layer for the subsequent epitaxial

growth of the long-range ordered thicker films with an hexagonal oxygen array of ~2.9 Å O-O distance. The reduction of O-O distance from ~3.0 Å for the 5 Å oxide overlayer or a diffused ring structure to ~2.9 Å for thicker aluminium oxide films is also accompanied by the substantial decrease of overlayer domain size from ~130 Å for the 5 Å oxide overlayer to 40-45 Å for thicker oxide films. To a good approximation, this reduction of O-O distance for thicker oxide films may undoubtly imply the formation of bulk-like aluminium oxide films gradually delivering the lattice mismatch-related strain (or stress) between the overlayer and the underlying substrate with the increase of the overlayer oxide thickness.

Prepared aluminium oxide overlayers are concluded to be chemically inert up to relatively high temperature regardless of the oxide thickness since no structural modifications are observed after the desorption of adsorbed methanol. The coverage-dependent thermal desorption spectra of the 5 Å interfacial layer as well as the 25 Å thick oxide film lead one to conclude that weak molecular chemisorption of methanol only occurs on well-oxidised, defectless aluminium oxide surfaces. The reliable leading edge analysis has revealed a desorption activation energy of 28-29 KJ/mol for extremely low methanol exposures on both alumina surfaces. The initial molecular adsorption is also supported by the the submonolayer (~0.83 ML) methanol coverage HREEL spectrum which is in close agreement with the previous vibrational spectra of solid methanol and molecularly adsorbed methanol on Al(111) and Al_2O_3 film on Ru(0001). This chemical inertness would be compatible with either model of the less-defective surface or the oxygen surface termination since the valence configuration of O^{2-} is fairly close to that of a rare gas then the surface oxygen layer should be rather inert with respect to reaction with closed shell molecules or electropositive reactants.

References

1. H.-J. Freund and E. Umbach, *Adsorption on Ordered Surfaces of Ionic Solids and Thin Films*, Vol. 33 (Springer-Verlag, Berlin, Heidelberg, 1993).
2. P. A. Cox, *Transition metal oxides: An introduction to their electronic structure and properties* (Clarendon Press, Oxford, 1995).
3. P. A. Cox, M. D. Hill, F. Peplinskii, and R. G. Egdell, Surf. Sci. **141**, 13 (1984).
4. R. G. Egdell, *Adsorption and Catalysis on Oxide Surfaces*, Ed. by M. Che and G. C. Bonds, p.173 (Elsevier Science Publishers B.V., Amsterdam, 1985).
5. P. A. Cox, R. G. Egdell, S. Eriksen, and W. R. Flavell, J. Electron Spectrosc. Relat. Phenom. **39**, 117 (1986).
6. S. Eriksen and R. G. Egdell, Surf. Sci. **180**, 263 (1987).
7. P. A. Cox and J. P. Kemp, Surf. Sci. **210**, 225 (1989).
8. H. Poelman, L. Fiermans, J. Vennik, and G. Dalmai, Surf. Sci. **275**, 351 (1992).
9. G. A. Sawatzky and D. Post, Phys. Rev. **B20**, 1546 (1979).
10. P. A. Cox, R. G. Egdell, C. Harding, W. R. Patterson, and P. J. Tavener, Surf. Sci. **123**, 179 (1982).
11. R. G. Egdell, H. Innes, and M. D. Hill, Surf. Sci. **149**, 33 (1985).
12. L. Kover, G. Moretti, Z. Kovacs, R. Sanjines, I. Cserny, G. Margaritondo, J. Palinkas, and H. Adachi, J. Vac. Sci. Technol. **A13**, 1382 (1995).
13. M. Baumer, D. Cappus, H. Kuhlenbeck, H.-J. Freund, G. Wilhelmi, A. Brodde, and H. Neddermeyer, Surf. Sci. **253**, 116 (1991).
14. T. Bertrams, A. Brodde, H. Hannemann, C. A. V. Jr, G. Wilhelmi, and H. Neddermeyer, *Adsorption on Ordered Surfaces of Ionic Solids and Thin Films*, Vol. 33, Ed. by H.-J. Freund and E. Umbachs, p.83 (Springer-Verlag, Berlin, Heidelberg, 1993).
15. L. H. Dubois, P. K. Hansma, and G. A. Somorjai, Appl. Surf. Sci. **6**, 173 (1980).
16. A. B. Stiles, Catalyst Support and Supported Catalysts (Butterworths, Boston, MA, 1987).
17. D. Venus, D. A. Hensley, and L. L. Kesmodel, Surf. Sci. **199**, 391 (1988).
18. D. A. King and D. P. Woodruff, *Adsorption at Solid Surfaces*, Vol. 2 (Elsevier Science Publishers B. V., Amsterdam, 1990).

19. P. J. Chen, M. L. Colaianni, and J. J. T. Yates, Phys. Rev. B41, 8025 (1990).
20. B. G. Frederick, G. Apai, and T. N. Rhodin, J. Am. Chem. Soc. **109**, 4797 (1987).
21. J. G. Chen, J. E. Crowell, and J. J. T. Yates, Surf. Sci. **187**, 243 (1987).
22. D. N. Belton and S. J. Schmieg, Surf. Sci. **199**, 518 (1988).
23. D. J. Hnatowich, J. Hudis, M. L. Perlman, and R. C. Ragaini, J. Appl. Phys. **42**, 4883 (1971).
24. G. Grimvall, Physica Scipta **9**, 43 (1974).
25. A. Balzarotti and A. Bianconi, Physica Status Solidi (b) **76**, 689 (1976).
26. G. H. Vurens, M. Salmeron, and G. A. Somorjai, Prog. Surf. Sci. **32**, 333 (1989).
27. H. Sambe and D. E. Ramaker, J. Vac. Sci. Technol. A**10**, 2991 (1992).
28. H. J. V. Beek and E. J. Mittemeijer, Thin Solid Films **122**, 131 (1984).
29. P. J. Chen and D. W. Goodman, Surf. Sci. **312**, L 767 (1994).
30. Y. Wu, E. Garfunkel, and T. E. Madey, J. Vac. Sci. Technol. A**14**, 2554 (1996).
31. M. B. Lee, B. G. Frederick, R. Bainbridge, and N. V. Richardson, *The 20th Anniversary Conference of the Korean Scientists and Engineers Association in the UK*, City, University of Oxford, Oxford, UK, 482 (1994).
32. M. B. Lee, Thesis, University of Liverpool, 1996.
33. R. Franchy, M. Wuttig, and H. Ibach, Surf. Sci. **189/190**, 438 (1987).
34. R. Franchy, J. Masuch, and P. Gassmann, Appl. Surf. Sci. **93**, 317 (1996).
35. P. Gassmann, R. Franchy, and H. Ibach, Surf. Sci. **319**, 95 (1994).
36. H. Isern and G. R. Castro, Surf. Sci. 211/212, 865 (1989).
37. R. M. Jaeger, H. Kuhlenbeck, H.-J. Freund, M. Wuttig, W. Hoffman, R. Franchy, and H. Ibach, Surf. Sci. **259**, 235 (1991).
38. J. P. Roux and H. J. Grabke, Appl. Surf. Sci. **68**, 49 (1993).
39. J. Libuda, F. Winkelmann, M. Baumer, H.-J. Freund, T. Bertrams, H. Neddermeyer, and K. Muller, Surf. Sci. **318**, 61 (1994).
40. J. F. Silvain, J. C. Bihr, M. Alnot, J. Lambert, and J. J. Ehrhardt, J. Vac. Sci. Technol. A**13**, 1893 (1995).
41. G. R. Castro, H. Isern, U. Schneider, M. Stocker, and K. Wandelt, Vacuum **41**, 393 (1990).
42. M. Bender, D. Ehrlich, I. N. Yakovkin, F. Rohr, M. Baumer, H. Kuhlenbeck, H. J. Freund, and V. Staemmler, J. Phys.: Cond. Matt. **7**, 5289 (1995).
43. F. W. McLafferty and D. B. Stauffer, *The Wiley/NBS Registry of Mass Spectral Data*, Vol. 1 (Wiley, 1989).
44. D. A. King, Surf. Sci. **47**, 384 (1975).
45. A. M. de Jong and J. W. Niemantsverdriet, Vacuum **41**, 1 (1990).
46. M. Falk and E. Whalley, J. Chem. Phys. **34**, 1554 (1961).
47. J. G. Chen, P. Basu, L. Ng, and J. J. T. Yates, Surf. Sci. **194**, 397 (1988).
48. B. G. Frederick, G. Apai, and T. N. Rhodin, Surf. Sci. **277**, 337 (1992).
49. D. R. Mullins and S. H. Overbury, Surf. Sci. **199**, 141 (1988).
50. H. L. Davis and J. R. Noonan, J. Vac. Sci. Technol. A**3**, 1507 (1985).
51. M. H. Kang and E. J. Mele, Phys. Rev. B**36**, 7371 (1987).
52. S. M. Yalisove and W. R. Graham, Surf. Sci. **183**, 556 (1987).
53. M. Wuttig, W. Hoffmann, E. Preub, R. Franchy, and H. Ibach, Vacuum **41**, 433 (1990).
54. D. R. Lide, *CRC Handbook of Chemistry and Physics*, Vol. 74 (CRC Press, Inc., Florida, 1993).
55. M. P. Seah and W. A. Dench, Surf. Interf. Anal. **1**, 2 (1979).
56. I. P. Batra and L. Kleinman, J. Electron Spectrosc. Relat. Phenom. **33**, 175 (1984).
57. H. Saalfeld, N. Jb. Miner., Abh. 95, 1 (1960).
58. K. Muller, H. Linder, D. M. Zehner, and G. Ownby, Verh. Dtsch. Phys. Ges., 1436 (1990).
59. M. H. Kang, S. C. Lui, E. J. Mele, E. W. Plummer, and D. M. Zehner, Phys. Rev. B**41**, 4920 (1990).
60. J. R. Heffelfinger, M. W. Bench, and C. B. Carter, Surf. Sci. **343**, L1161 (1995).
61. G. Ertl and J. Kuppers, *Low Energy Electrons and Surface Chemistry*, p. 201 (VCH, Weinheim, 1985).
62. T. Matsushima and J. M. White, Journal of Catalysis **44**, 183 (1976).
63. I. F. Tindall and J. C. Vickerman, Surf. Sci. **149**, 577 (1985).
64. E. Habenschaden and J. Kuppers, Surf. Sci. Lett. **138**, L147 (1984).